Application of Multipoint Measurements for Flow Characterization

Mark N. Glauser
Department of Mechanical and Aeronautical Engineering, Clarkson University, Potsdam, New York

William K. George
Department of Mechanical and Aerospace Engineering, State University of New York at Buffalo, Buffalo, New York

■ Some of the possibilities for inferring the structure of complicated flows from simultaneous measurements at many points are reviewed. Conditional sampling, pseudo-flow visualization, stochastic estimation, and the proper orthogonal decomposition are briefly reviewed and illustrated by example. Resolution criteria for multipoint spatial arrays are proposed that minimize the possibilities for misinterpreting the data.

Keywords: *spatial and temporal aliasing, conditional measurements, pseudo-flow visualization, stochastic estimation, proper orthogonal decomposition, periodic and homogeneous fields, inhomogeneous fields, windowing*

INTRODUCTION

One of the most important tools of the fluid dynamicist is the ability to visualize the fluid motions in the problem of interest. Flow visualization by tagging fluid material has a long and rich history and has stimulated scientist, engineer, and artist alike. Many a student, not to mention experienced investigator, has been fascinated by the crisp and revealing motion pictures of the NSF Fluid Mechanics Film series [1]. More than one has wished that he had the capability of revealing the details of his own flow with simple dye, smoke, or hydrogen bubble experiments. But alas! It is an unfortunate fact of nature that the same fluids whose mysterious motions we seek to unravel, conspire through molecular diffusion and other processes to invalidate these simple tools. Thus most have had to recognize the futility of such efforts in a large number of flow environments and have had to settle for far, far less information about what the flow is really doing. (The photo collection by Van Dyke [2] is proof, however, that at least a few have succeeded.)

For the experimentalist, this has usually meant settling for measurements of the average properties of the flow at a relatively small number of points in it. These limited experimental capabilities have undoubtedly had a negative effect on the efforts of theoreticians, because of both the lack of possibility for comparison with experimental data and the failure to overturn theories that were incorrect. One need only witness the role being played by supercomputer simulations of flows (in combustion, for example) to realize what might have been had not the experimentalist had to settle for so little. Happily, for the experimentalist at least, it will be some time before full Navier–Stokes simulations of most engineering problems will become possible.

But the CFD community has not been the only one to benefit from the technical advances in hardware. One of the opportunities presented by the advances in electronics and computers over the past two decades is the possibility of making many measurements at many points in the flow simultaneously. Experiments utilizing tens of probes together have become routine, and now experiments using hundreds of probes are in the planning stage or in progress. The transducers vary from thin-film gauges to hot wires, from optical scanners to holographic interferometry; and the flow environments vary from gas turbines to trees (Yes, real trees with branches and leaves!), from boundary layers to combustion chambers. All have a common objective: to obtain by computer imaging and statistical means a picture of what is really happening.

It is not our intent in this paper to provide a review of the variety of efforts hinted at above. Nor is it our intent to review the multiplicity of transducers that can be used for multipoint measurements. Instead, the focus will be twofold:

1. To demonstrate how measurements at many points can be used to infer the structure of the flow
2. To decide what constraints must be placed on the measurements to ensure that proper interpretation is possible

The first objective will be approached by a brief review of four basic techniques for handling multipoint data: conditional sampling, pseudo-flow visualization, stochastic estimation, and the proper orthogonal decomposition. To appreciate the need for these, one must understand the character of high Reynolds number, often turbulent, motions. As modern full Navier–Stokes computer simulations have made clear, a knowledge of the data at many points in the flow does little in and of itself to make clear what is happening because of the chaotic nature of the flow. The key to understanding usually lies in what is done to the data to bring the underlying order (we hope it's order) to

Address correspondence to Professor Mark N. Glauser, Department of Mechanical and Aeronautical Engineering, Clarkson University, Potsdam, NY 13699.

Experimental Thermal and Fluid Science 1992; 5:617–632

0894-1777/92/$5.00

the foreground. The four techniques chosen for discussion have found wide utilization over the past decade, and all hold forth the promise of extensive application in the future. All four will be illustrated by examples from the literature. Although the examples chosen all involve applications of hot-wire anemometry, there is nothing intrinsic to the techniques under discussion that limits their application. Thus they can be applied to any multipoint transducer array in most environments.

The second objective will be to provide resolution criteria for multipoint flow measurements. This is necessary if the purpose of the experiment is not to simply facilitate taking large quantities of single-point data, but rather to enable understanding the flow's spatial and temporal structure. This resolution objective will be accomplished by first reviewing the requirements for single-point measurements, then extending these requirements to include the constraints on spatial arrays in various environments. The goal (only partially realized) is to place the theory of spatial sampling at the same level of understanding as that for the digital sampling of time series. Although it will be necessary and convenient to represent the signals by their Fourier and proper orthogonal decompositions (for homogeneous and inhomogeneous flows, respectively), the results are believed to have wide applicability to all kinds of multipoint measurements, especially when used in conjunction with the interpretation techniques described above.

TECHNIQUES FOR IDENTIFYING FLOW STRUCTURE

The use of rakes of probes with good spatial resolution presents the opportunity to examine the structure of turbulent flowfields in ways that would not otherwise be possible. In this section several approaches will be discussed. The first involves using the simultaneous velocities obtained from rakes of hot wires in conjunction with conditional sampling techniques. The second, termed pseudo-flow visualization (PFV), consists of using the simultaneous velocity measurements obtained with hot-wire rakes to generate instantaneous velocity profiles. From these profiles the spatial extent and characteristic frequencies of the large-scale structures can be determined. The third and fourth approaches involve the use of the simultaneous velocities in conjunction with stochastic estimation and proper orthogonal decomposition techniques.

Conditional Measurements

Simultaneous measurement using rakes of hot-wire probes have been used in conjunction with conditional sampling techniques by numerous authors to examine the large-scale features of turbulent flows. These investigations have helped shed new light on the turbulence structure in a variety of flows including wakes, jets, free shear layers, and boundary layers. In the following paragraphs, several examples have been chosen as illustrative; no attempt has been made, however, to provide a comprehensive review of the numerous applications.

In one of the first extensive applications of rakes of hot wires, Blackwelder and Kaplan [3] examined the wall structure of the turbulent boundary layer using conditional sampling techniques. They used the two different rakes shown in Figs. 1 and 2, the first to examine the instantaneous variation of the streamwise velocity in the direction normal to the flat plate and the other to examine the instantaneous variation in the spanwise direction. They found that the instantaneous streamwise velocity measurements normal to the wall exhibited a high degree of coherence over a large area in the direction normal to the wall. They also found from the spanwise rake measurements that there was evidence of a large-scale correlation in the spanwise direction farther out in the boundary layer ($y^+ = 15$) but no evidence of the streaks that are apparent (from flow visualization studies) in the lower regions of the boundary layer. From their conditional measurements they concluded that the normal velocity was directed outwards in regions of strong streamwise momentum deficit, and inwards when the streamwise velocity exceeded its mean value.

Teitel and Antonia [4] used an array of cross-wire probes in a fully developed turbulent duct flow. The rakes were deployed in the plane of mean shear to examine the interaction between the opposite shear layers, providing *simultaneous* information on the turbulence characteristics of the shear layers on either side of the centerline. A significant finding of their work was that instantaneous quadrant 2 events (u negative and v positive) on one side of the centerline can almost reach the opposite wall. It should be noted that this information was obtainable only from a rake of wires. They then argued that the contribution from quadrant 2 events to the Reynolds shear stress is smaller in duct flow than in a boundary layer, reflecting the mutually inhibiting effect of the flow structures associated with the opposite shear layers. Antonia and his colleagues (see Antonia et al [5]) used a similar arrangement to examine the turbulent far wake of a circular cylinder. They were able to identify, using an array of eight cross-wires, structures that were both symmetric and antisymmetric about the centerline.

The spanwise structure in the two-dimensional mixing layer was examined by Browand and Troutt [6]. They used a rake of 12 hot wires across the span of the wind tunnel.

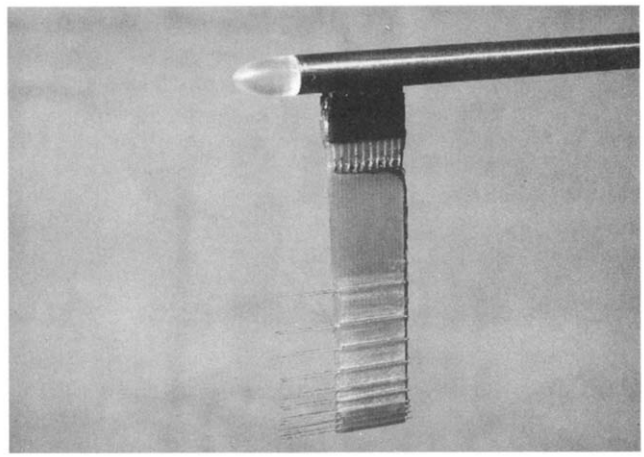

Figure 1. Rake used by Blackwelder and Kaplan to examine direction normal to flat plate.

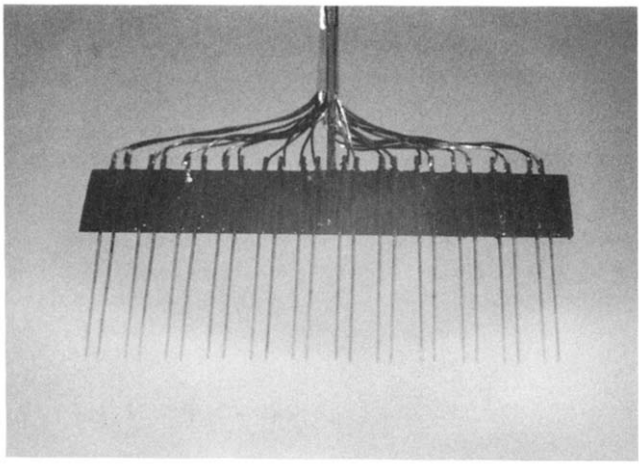

Figure 2. Rake used by Blackwelder and Kaplan to examine spanwise direction.

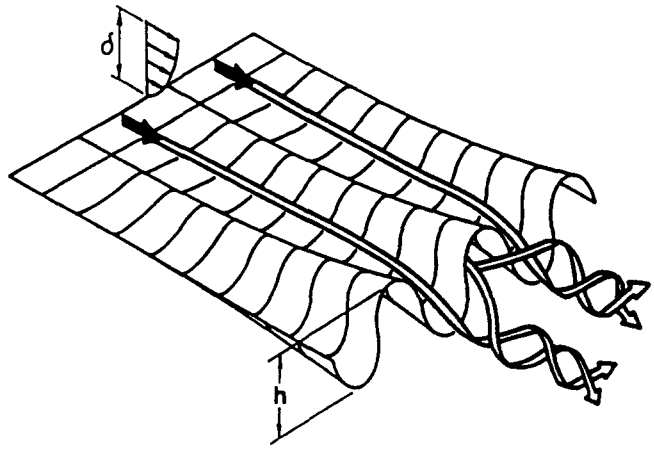

Figure 3. Lobed mixer enhancing streamwise vorticity.

Computer visualizations of the instantaneous hot-wire outputs showed that the large-scale structures extended across the wind tunnel and that there was some spanwise irregularity. They inferred from this that the spanwise irregularity is related to interactions between adjacent vortices.

Hussain and his colleagues at Houston (see Hussain [7]) have developed a technique for the "eduction" of structure that requires a rake of cross-wires. From these rakes they record the instantaneous velocity traces. They then smooth these traces via short-time averaging and infer the time evolution of "pseudo-vorticity" contours in the plane of the sensors. (Note that actual vorticity measurement would have required substantially greater resolution than was possible in the experiment.) Others, such as Nagib and his coworkers at Illinois Institute of Technology (H. Nagib, private communication, 1982), have used rakes of wires to study transition in various flows.

Pseudo-Flow Visualization

All of the examples cited above plotted simultaneous velocity traces to gain insight into turbulent flows. This has recently been extended to a technique called *pseudo-flow visualization* (PFV), first termed this by Tabatabai et al [8] and detailed by Delville et al [9]. PFV utilizes hot-wire rakes with high spatial resolution to create a graphical representation of the instantaneous velocity profiles in a flowfield. A sense of the streamwise spatial variation is conveyed for convected flows by the simultaneous display of the time histories of the measurements at each point. These should be interpreted with due regard for the validity (or lack of it) of Taylor's hypothesis (see Lumley [10] and Zaman and Hussain [11]). Since conventional flow visualization techniques break down at high Reynolds numbers owing to turbulent diffusion, pseudo-flow visualization methods provide an alternative technique for visualizing the flowfield in such cases.

The PFV method can be illustrated by the recent studies of Ukeiley et al [12], who examined the turbulent flow in a lobed mixer, a device for increasing mixing by enhancing streamwise vorticity (see Fig. 3). A rake of single-component hot wires (Ukeiley et al [13]) was used to collect a record of the instantaneous streamwise velocity–time traces at several positions simultaneously. The rake contained 15 probes, each having a 5 μm tungsten wire with a sensing length of 1 mm. The rake spanned a full lobe width with a hot-wire separation distance of 2.7 mm. In spite of the scope of the experiment, it was possible to collect the data with a personal computer data acquisition system.

Traditional analysis of hot-wire data involves plotting the instantaneous velocities at one location in space. However, a rake of hot wires allows instantaneous velocities across the spatial extent of the rake to be plotted at each sampled time interval, thereby permitting insight into the relationships among all the measurements as time evolves. Figure 4 demonstrates the comparison between the PFV and the more traditional way of plotting instantaneous velocities.

PFV plots were created at five positions across the center lobes at each of three locations, 50, 100, and 150 mm downstream of the lobed mixer (refer to Figs. 5 and 6). Figures 7–9 display the results obtained at these spatial locations. At 50 mm downstream there are discernible differences among the five visualizations. Positions 2 and 4 show minimal fluctuations and small gradients, while positions 1, 3, and 5 are strongly indicative of the shear regions created by the lobes. At 100 mm downstream, visualizations of positions 1, 3, and 5 indicate further development of these shear regions, while positions 2 and 4 show the beginning development of interactions between the two streams. By 150 mm downstream there is almost no difference in the PFV patterns for all five positions. This last set of pseudo-flow visualizations suggest an increase in turbulence mixing, presumably at the expense of the mean streamwise vortices that have been shown by Eckerle et al [14] to begin to decay in this downstream region. Figure 10 shows the comparison of the PFV to a spectral measurement at position 1, 50 mm downstream of this lobed mixer. The approximate number of structures counted in the PFV plot corresponds with the frequency of occurrence of these structures as determined from the spectrum to be approximately 700 Hz.

This method was also applied by Delville et al [9] to a study of the structures in a turbulent, plane mixing layer.

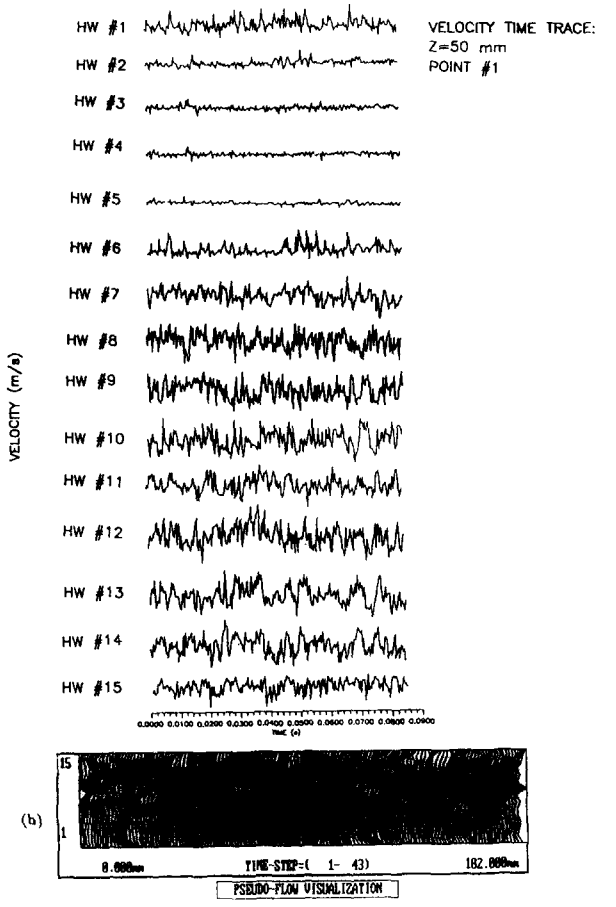

Figure 4. (*a*) Conventional velocity–time traces. (*b*) Sample pseudo-flow visualization plot.

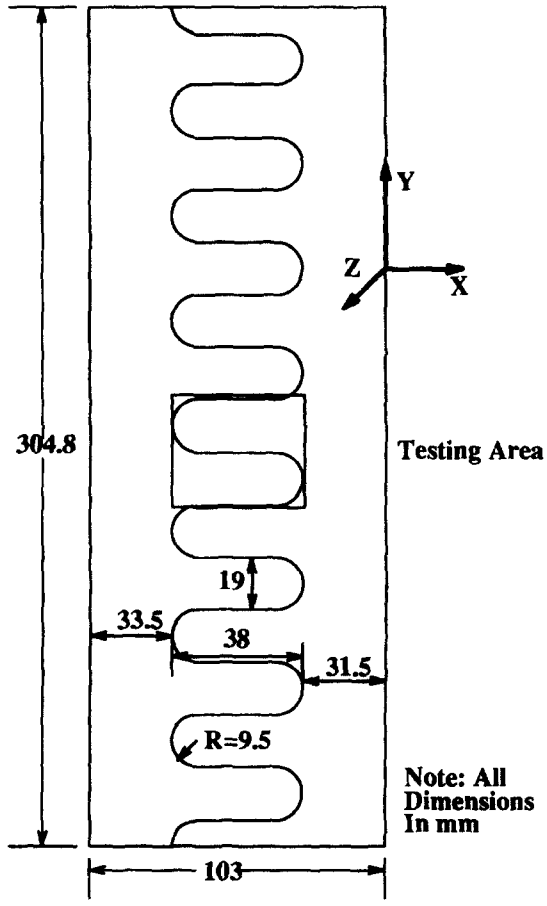

Figure 5. Test section.

From the instantaneous velocity profiles, detailed structures were observed in both the transverse and spanwise directions. Delville et al were then able to use an edge extraction scheme to find an intermittency function that corresponded to the passage of the structures. From these results they found the spanwise to streamwise wavelength ratio to be approximately 0.16.

It should be noted that the structures observed using the PFV technique in both experiments would be much more difficult (if not impossible) to infer from real flow visualization techniques owing to turbulent diffusion effects at the relatively high speeds used in these studies. The Ukeiley et al [12] study demonstrates that the hot-wire rake based PFV technique provides a simple and effective means for determining how well devices such as the lobed mixer perform, and that it potentially has many applications in industry. The limitations of the PFV technique in its present form are spatial aliasing (discussed later) and its inability to capture three-dimensional instantaneous structure.

Stochastic Estimation

One of the more popular ideas in experimental turbulence at present is that of stochastic estimation, which provides a means for quantifying large-scale structures in turbulent flows (see Adrian and Moin [15] and references therein). In brief, stochastic estimation uses knowledge of a field at one or more points together with its statistical properties to infer its "typical" behavior at other locations. Only

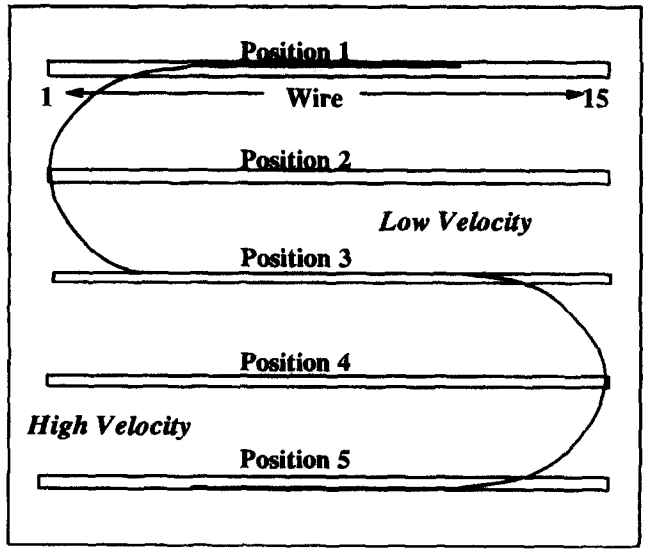

Figure 6. Positions for data collection.

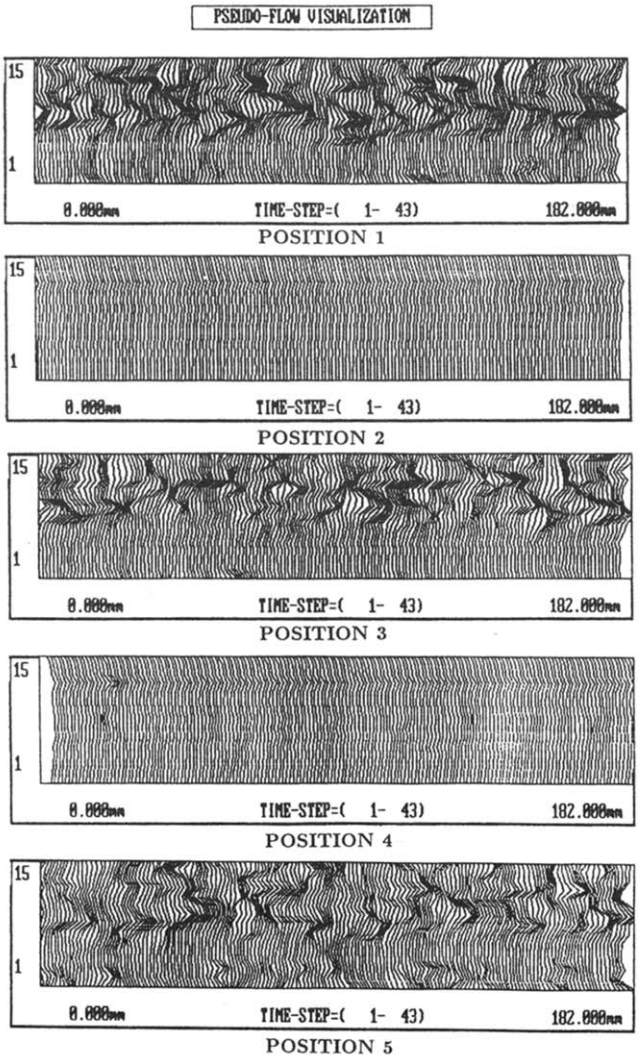

Figure 7. Pseudo-flow visualization plots at 50 mm downstream.

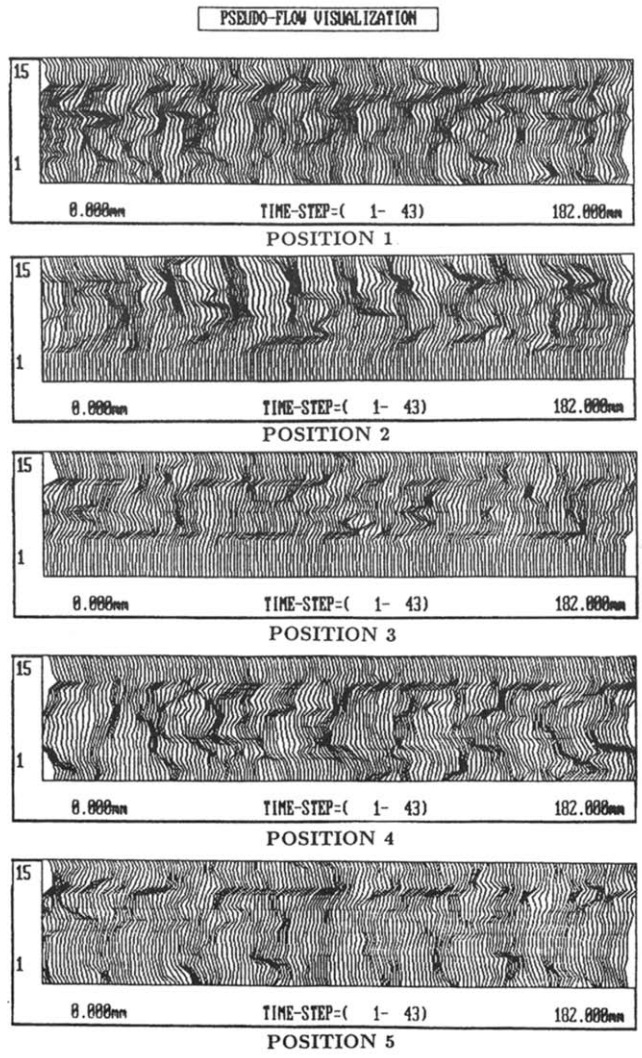

Figure 8. Pseudo-flow visualization plots at 100 mm downstream.

linear stochastic estimation (LSE) will be discussed here, as Tung and Adrian [16] have shown that little is to be gained by going to second order or higher. Application of this technique requires knowledge of the two-point correlation tensor which can be obtained with only two probes. The conditional eddy can be estimated using various averaged quantities (for example, the Reynolds stress) to provide the condition. The use of rakes of probes, however, provides many more possibilities for estimating the simultaneous velocity vector field using the instantaneous velocities at one or more points across the span.

A conditional average can be defined as

$$\langle g(u)|E\rangle = \text{expected value of } g(u) \tag{1}$$

given that the event E, the detector of the coherent structure, occurs. However, since the properties of these coherent structures are not known beforehand, it is difficult to determine reliable unambiguous and unbiased detector events. Adrian [17] suggested choosing

$$g(u) = u(x') \tag{2}$$

and

$$E = c \leq u(x) < c + dc \tag{3}$$

which confines the velocity to a small window between c and $c + dc$, where c is any arbitrary vector. Symbolically,

$$\tilde{u}(x') = \langle u(x')|u(x)\rangle \tag{4}$$

which can be approximated, for the linear estimate, as

$$\tilde{u}_i(x') = A_{ij}u_j(x) \tag{5}$$

Values for the coefficients A_{ij} are chosen such that the mean-square error is minimized as

$$e_i = \left\langle [\tilde{u}_i(x') - \langle u_i(x')|u(x)\rangle]^2 \right\rangle \tag{6}$$

for $i = 1, 2, 3$. This minimization requires that

$$\frac{\partial e_i}{\partial A_{ij}} = 0 \tag{7}$$

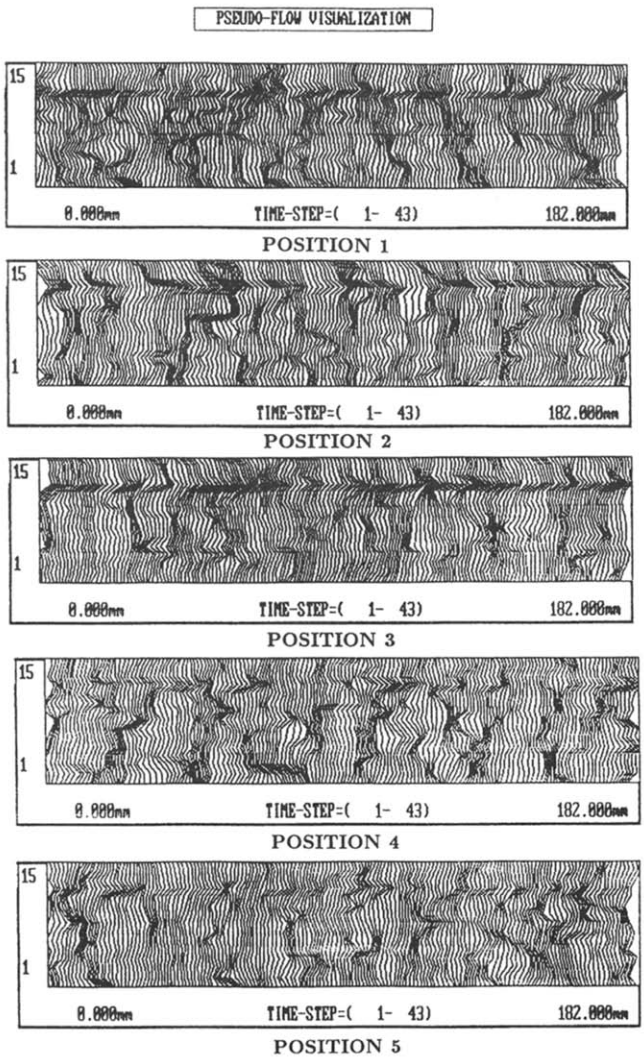

Figure 9. Pseudo-flow visualization plots at 150 mm downstream.

which leads to an equation of the form

$$\langle u_j(x)u_k(x)\rangle A_{ik} = \langle u_j(x)u_i(x')\rangle \qquad (8)$$

where $\langle u_j(x)u_k(x)\rangle$ is the Reynolds stress tensor and $\langle u_j(x)u_i(x')\rangle$ is the two-point correlation tensor.

These ideas can be illustrated using the recent application of LSE to the axisymmetric jet mixing layer by Cole et al [18, 19]. This work differs from previous studies in that the *instantaneous* velocities at more than one position across the jet shear layer provided the events. The simultaneous velocity and two-point correlation tensor data of Glauser and George [20] were used for this application. In their high Reynolds number experiment (Re = 100,000), eight cross-wires, spanning radially across the jet mixing layer at $x/D = 3$, were used to simultaneously measure the streamwise and radial velocities. The rakes were constructed on printed circuit boards similar in design to those used by Nagib and his colleagues at IIT and are described in Glauser [21].

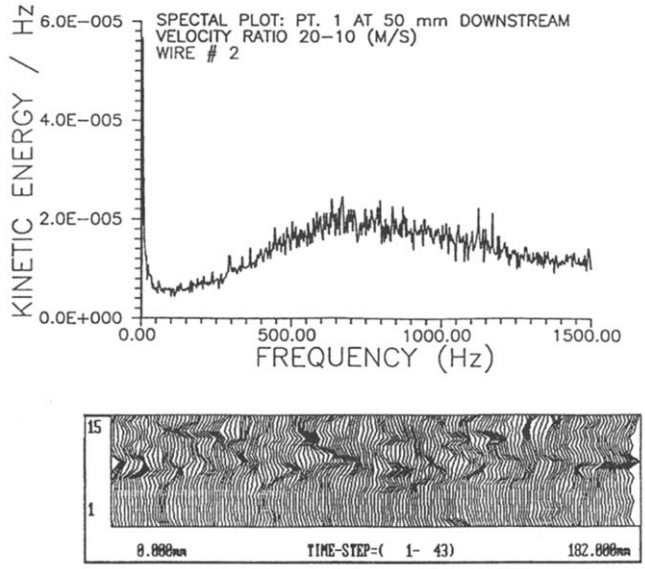

Figure 10. Comparison of pseudo-flow visualization to energy spectrum.

Expanding Eq. (8) results in the following system of equations for the u, v data of Glauser and George [20].

First System

$$\begin{vmatrix} \langle u^2\rangle & \langle uv\rangle \\ \langle vu\rangle & \langle v^2\rangle \end{vmatrix} \begin{vmatrix} A_{11} \\ A_{12} \end{vmatrix} = \begin{vmatrix} \langle uu'\rangle \\ \langle uv'\rangle \end{vmatrix}$$

Second System

$$\begin{vmatrix} \langle u^2\rangle & \langle uv\rangle \\ \langle vu\rangle & \langle v^2\rangle \end{vmatrix} \begin{vmatrix} A_{21} \\ A_{22} \end{vmatrix} = \begin{vmatrix} \langle vu'\rangle \\ \langle vv'\rangle \end{vmatrix}$$

The estimated velocity components are now obtained by expanding Eq. (5), which results in

$$\tilde{u} = A_{11}u + A_{12}v, \qquad \tilde{v} = A_{21}u + A_{22}v$$

After this technique is applied to the data of Glauser and George [20], the matrices that arise for a *single*-wire estimate are as follows.

First System

$$\begin{vmatrix} \langle u_{\text{ref}}^2\rangle & \langle u_{\text{ref}}v_{\text{ref}}\rangle \\ \langle v_{\text{ref}}u_{\text{ref}}\rangle & \langle v_{\text{ref}}^2\rangle \end{vmatrix} \begin{vmatrix} A_{11w} \\ A_{12w} \end{vmatrix} = \begin{vmatrix} \langle u_{\text{ref}}u_w\rangle \\ \langle u_{\text{ref}}v_w\rangle \end{vmatrix}$$

Second System

$$\begin{vmatrix} \langle u_{\text{ref}}^2\rangle & \langle u_{\text{ref}}v_{\text{ref}}\rangle \\ \langle v_{\text{ref}}u_{\text{ref}}\rangle & \langle v_{\text{ref}}^2\rangle \end{vmatrix} \begin{vmatrix} A_{11w} \\ A_{12w} \end{vmatrix} = \begin{vmatrix} \langle v_{\text{ref}}u_w\rangle \\ \langle v_{\text{ref}}v_w\rangle \end{vmatrix}$$

where ref is the reference wire number and w is the wire number (ie, 1–8 in this case).

For a *two*-wire estimate, these matrices become

First System

$$\begin{vmatrix} \overline{u_{\mathrm{ref}_1}^2} & \overline{u_{\mathrm{ref}_1}v_{\mathrm{ref}_1}} & \overline{u_{\mathrm{ref}_1}u_{\mathrm{ref}_2}} & \overline{u_{\mathrm{ref}_1}v_{\mathrm{ref}_2}} \\ \overline{v_{\mathrm{ref}_1}u_{\mathrm{ref}_1}} & \overline{v_{\mathrm{ref}_1}^2} & \overline{v_{\mathrm{ref}_1}u_{\mathrm{ref}_2}} & \overline{v_{\mathrm{ref}_1}v_{\mathrm{ref}_2}} \\ \overline{u_{\mathrm{ref}_2}u_{\mathrm{ref}_1}} & \overline{u_{\mathrm{ref}_2}v_{\mathrm{ref}_1}} & \overline{u_{\mathrm{ref}_2}^2} & \overline{u_{\mathrm{ref}_2}v_{\mathrm{ref}_2}} \\ \overline{v_{\mathrm{ref}_2}u_{\mathrm{ref}_1}} & \overline{v_{\mathrm{ref}_2}v_{\mathrm{ref}_1}} & \overline{v_{\mathrm{ref}_2}u_{\mathrm{ref}_2}} & \overline{v_{\mathrm{ref}_2}^2} \end{vmatrix} \begin{vmatrix} A_{11w}^{\mathrm{ref}_1} \\ A_{12w}^{\mathrm{ref}_1} \\ A_{11w}^{\mathrm{ref}_2} \\ A_{12w}^{\mathrm{ref}_2} \end{vmatrix} = \begin{vmatrix} \overline{u_{\mathrm{ref}_1}u_w} \\ \overline{u_{\mathrm{ref}_1}v_w} \\ \overline{u_{\mathrm{ref}_2}u_w} \\ \overline{u_{\mathrm{ref}_2}v_w} \end{vmatrix}$$

Second System

$$\begin{vmatrix} \overline{u_{\mathrm{ref}_1}^2} & \overline{u_{\mathrm{ref}_1}v_{\mathrm{ref}_1}} & \overline{u_{\mathrm{ref}_1}u_{\mathrm{ref}_2}} & \overline{v_{\mathrm{ref}_1}u_{\mathrm{ref}_2}} \\ \overline{v_{\mathrm{ref}_1}u_{\mathrm{ref}_1}} & \overline{v_{\mathrm{ref}_1}^2} & \overline{v_{\mathrm{ref}_1}u_{\mathrm{ref}_2}} & \overline{v_{\mathrm{ref}_1}v_{\mathrm{ref}_2}} \\ \overline{u_{\mathrm{ref}_2}u_{\mathrm{ref}_1}} & \overline{u_{\mathrm{ref}_2}v_{\mathrm{ref}_1}} & \overline{u_{\mathrm{ref}_2}^2} & \overline{u_{\mathrm{ref}_2}v_{\mathrm{ref}_2}} \\ \overline{v_{\mathrm{ref}_2}u_{\mathrm{ref}_1}} & \overline{v_{\mathrm{ref}_2}v_{\mathrm{ref}_1}} & \overline{v_{\mathrm{ref}_2}u_{\mathrm{ref}_2}} & \overline{v_{\mathrm{ref}_2}^2} \end{vmatrix} \begin{vmatrix} A_{21w}^{\mathrm{ref}_1} \\ A_{22w}^{\mathrm{ref}_1} \\ A_{21w}^{\mathrm{ref}_2} \\ A_{22w}^{\mathrm{ref}_2} \end{vmatrix} = \begin{vmatrix} \overline{v_{\mathrm{ref}_1}u_w} \\ \overline{v_{\mathrm{ref}_1}v_w} \\ \overline{v_{\mathrm{ref}_2}u_w} \\ \overline{v_{\mathrm{ref}_2}v_w} \end{vmatrix}$$

where ref_1 and ref_2 are reference wires 1 and 2, respectively, and the overbar is used here to denote an averaged quantity to save space. The estimates for the two-wire reference case are then

$$\tilde{u}_w = A_{11w}^{\mathrm{ref}_1}u_{\mathrm{ref}_1} + A_{12w}^{\mathrm{ref}_1}v_{\mathrm{ref}_1} + A_{11w}^{\mathrm{ref}_2}u_{\mathrm{ref}_2} + A_{12w}^{\mathrm{ref}_2}v_{\mathrm{ref}_2} \quad (9)$$

and

$$\tilde{v}_w = A_{21w}^{\mathrm{ref}_1}u_{\mathrm{ref}_1} + A_{22w}^{\mathrm{ref}_1}v_{\mathrm{ref}_1} + A_{21w}^{\mathrm{ref}_2}u_{\mathrm{ref}_2} + A_{22w}^{\mathrm{ref}_2}v_{\mathrm{ref}_2} \quad (10)$$

Without much trouble this system can easily be expanded to include estimates of all eight wires. An obvious property of the eight-wire estimate is that the estimated velocities will be exactly the same as the actual velocities.

Cole et al [18, 19] have estimated the velocity field using various reference positions for both single-point and multipoint estimates. A time record of the original velocity vectors at the eight radial positions across the jet shear layer at $x/D = 3$ is shown plotted in Fig. 11. Figures 12, 13, and 14 show the single-point estimated fields using wires 3, 4, and 5, respectively, as reference. These were constructed using the single-point versions of Eqs. (9) and (10). Note the large differences between these conditional estimates and how they differ from the original vector field. It is clear that a one-point reconstruction *does not* do an adequate job of estimating the entire flow. How-

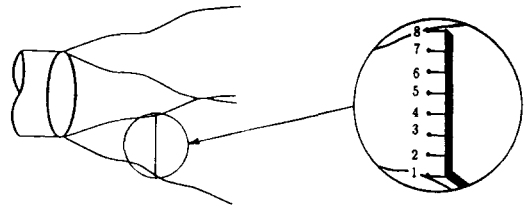

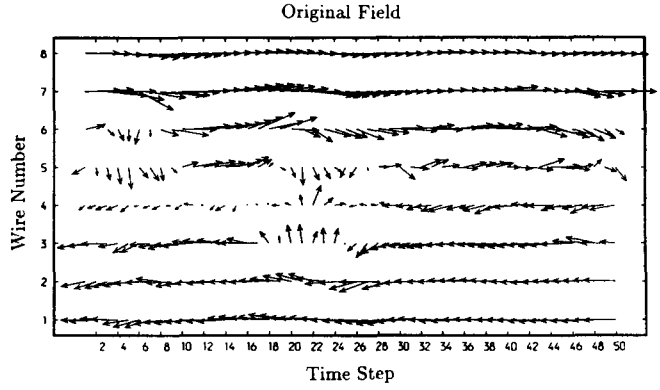

Figure 11. Instantaneous velocity vector plots seen in a frame of reference moving at U_c = 12 m/s. Each time step is 0.0005 s, and the spacing between the wires is 1.09 cm. Note the positioning of the wires in the jet shear layer.

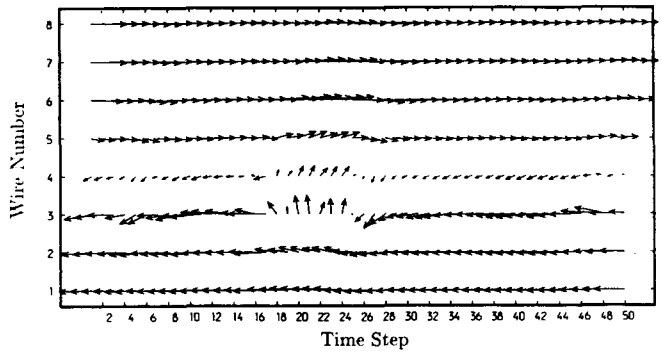

Figure 12. Estimated field using reference wire 3.

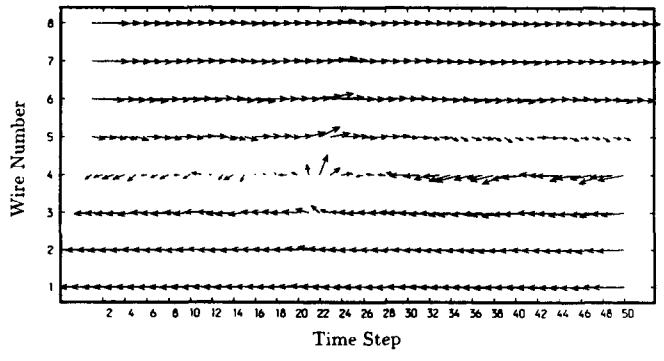

Figure 13. Estimated field using reference wire 4.

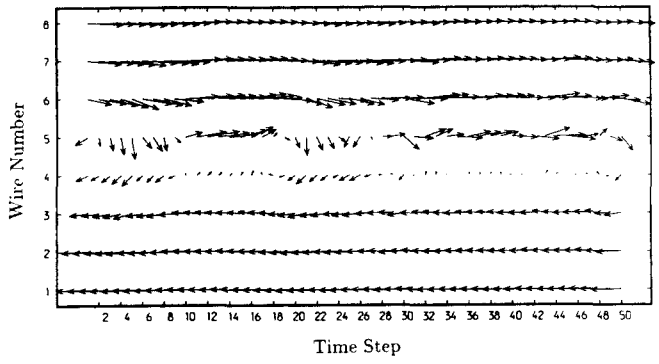

Figure 14. Estimated field using reference wire 5.

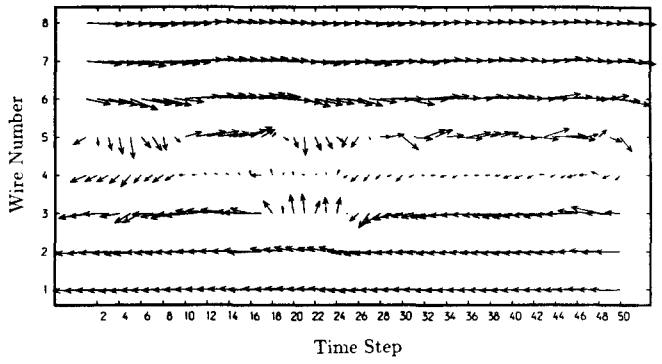

Figure 15. Estimated field using reference wires 3 and 5.

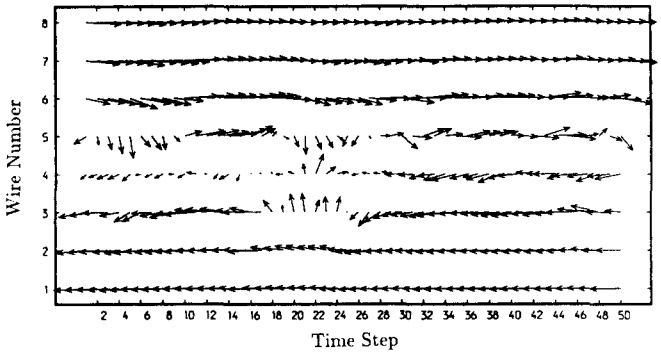

Figure 16. Estimated field using reference wires 3, 4, and 5.

ever, the conditional estimates obtained using wires located just off either side of the centerline of the shear layer do a reasonable job in reconstructing the other wires located on the same side but capture very little from the opposite side of the shear layer.

Since the one-point conditional estimates clearly bias the eddy detected, multipoint estimates were used by Cole et al [18, 19] to try to capture a more representative instantaneous conditional eddy. Figures 15 and 16 show estimates obtained using reference wires 3 and 5 and wires 3, 4, and 5, respectively. These were constructed using Eqs. (9) and (10) for the two-wire estimates and a three-wire version for the three-wire estimates. Note how much better these results compare to one another and to the original random velocity field shown in Fig. 11. From these results the authors conclude that a two-point reconstruction (specifically wires 3 and 5) does an adequate job in reconstructing the entire flow and that little is gained by going to a three-point estimate. They also demonstrate that for computing conditional averages the number and proper placement of the reference probes are critical.

Proper Orthogonal Decomposition

Another popular idea for characterizing flow structures in turbulence is the so-called proper orthogonal decomposition (POD). Like stochastic estimation, POD requires knowledge of the two-point correlation tensor. This can be obtained from two-point measurements alone, so that if one is interested only in reconstructing averaged quantities such as spectra then the two-point measurements are sufficient. If, however, the full power of the POD is to be exploited to reconstruct the instantaneous decomposed velocity fields, then rakes of hot wires must be used. As will be shown later, this latter possibility presents opportunities for using the PFV technique to visualize the results of POD.

POD results from the search for a deterministic field that has the largest mean-square projection on the velocity field (ie, the structure that maximizes the energy; see Lumley [22]). Maximizing the mean-square projection leads to the integral eigenvalue problem

$$\iiiint R_{ij}(\boldsymbol{x},\boldsymbol{x}',t,t')\phi_j^{(n)}(\boldsymbol{x}',t')\,d\boldsymbol{x}'\,dt' = \lambda^{(n)}\phi_i^{(n)}(\boldsymbol{x},t) \tag{11}$$

The kernel of Eq. (11) is the two-point velocity cross-correlation tensor, $R_{ij}(\boldsymbol{x},\boldsymbol{x}',t,t') = \langle u_i(\boldsymbol{x},t)u_j(\boldsymbol{x}',t')\rangle$, and the summation of the eigenvalues is equal to the total energy. The integral equation has an infinite number of orthogonal solutions that can be used to reconstruct the original random velocity by the equation

$$u_i(\boldsymbol{x},t) = \sum_{n=1}^{\infty} a_n\phi_i^{(n)}(\boldsymbol{x},t) \tag{12}$$

where the coefficients a_n are random and uncorrelated and must be determined for each realization of the flow by projecting the eigenfunctions on it.

If a direction (or time) is assumed to be statistically stationary, homogeneous, or periodic, the POD reduces to the more familiar harmonic decomposition so that Fourier analysis is used in these directions (see George [23]). Assuming the flow to be homogeneous in the streamwise direction z and stationary in time, Eq. (11) reduces to

$$\int \Phi_{ij}(x,x',y,y',f,k_1)\psi_j^{(n)}(x',y',f,k_1)\,dx'\,dy' = \lambda^{(n)}(k_1,f)\psi_i^{(n)}(x,y,f,k_1) \tag{13}$$

where $\Phi_{ij}(x,x',y,y',f,k_1)$ is the Fourier transform of $R_{ij}(x,x',t,t')$ in the stationary and homogeneous directions. The ψ's are the frequency- and wavenumber-dependent eigenfunctions, and x and y denote the remaining inhomogeneous directions (see Fig. 5). Note that often it is convenient to treat an inhomogeneous but slowly developing flow as if it were locally homogeneous in the

streamwise direction, as in the lobed mixer experiment discussed earlier and below.

Simpler decompositions using only some of the variables can also be used. For example, Ukeiley et al [12] considered the reduced decomposition given by

$$\int \Phi_{11}(x, x', f)\psi_1^{(n)}(x', f)\, dx' = \lambda^{(n)}(f)\psi_1^{(n)}(x, f) \quad (14)$$

where Φ_{11} is the measured one-dimensional spectrum across the flow. In Eq. (14), only the spanwise direction, x, is decomposed through the use of POD. The vertical direction, y, is also statistically inhomogeneous in this flow but is not considered in this preliminary examination. The streamwise velocity component that has been decomposed with Fourier analysis can be reproduced in Fourier space by

$$\hat{u}_1(x, f) = \sum_{n=1}^{\infty} a_n(f)\psi_1^{(n)}(x, f) \quad (15)$$

where the random coefficients $a_n(f)$ can be calculated for a single realization of the transformed field by

$$a_n(f) = \int \hat{u}_1(x, f)\psi_1^{(n)*}(x, f)\, dx \quad (16)$$

This equation is derived by a process similar to that of a Fourier decomposition [ie, multiplying Eq. (15) by ψ^*, where the $*$ denotes the complex conjugate, and integrating over the whole region].

The numerical approximation, detailed by Glauser et al [24], simply consists of replacing the integral in Eq. (14) by an appropriate quadrature rule (in this study a trapezoidal rule). $\Phi_{11}(x, x', f)$ is obtained from experimental measurements and used in Eq. (14) to obtain the eigenvalues and eigenfunctions. These eigenfunctions are then used to reconstruct the original Fourier-transformed random velocity field. This streamwise velocity component in Fourier space can then be inverse-transformed to obtain the reconstructed instantaneous velocity–time trace. It should be noted that the random coefficients could *not* have been calculated if rakes of hot wires had not been used. This is because the instantaneous velocity at all points x are needed simultaneously so that the integral in Eq. (16) can be computed.

Figure 17 illustrates pseudo-flow visualization plots of reconstructed instantaneous signals for various proper orthogonal modes of the lobed mixer flow as reported by Ukeiley et al [12]. The contribution from the first eigenmode, displayed in Fig. 17*b*, shows a good representation of the dominant structures shown in Fig. 17*a*. The first three eigenmodes combined capture the *global* features seen in the pseudo-flow visualization of the total streamwise velocity field as illustrated in Fig. 17*c*. The summation of the first five modes displayed in Fig. 17*d* reproduces the general shape of the original plot at all locations. However, the smaller scales are not completely captured. A summation of the first seven eigenmodes is needed to obtain a reconstruction that captures the small scales, as seen by comparing Figs. 17*a* and 17*e*. The contributions from subsequent modes are negligible. One can argue from these results that the large-scale features of this flowfield can be adequately represented by using the first proper orthogonal mode alone. These results indicate that a low dimensional dynamical systems approach may be fruitful for this flow, [25, 26].

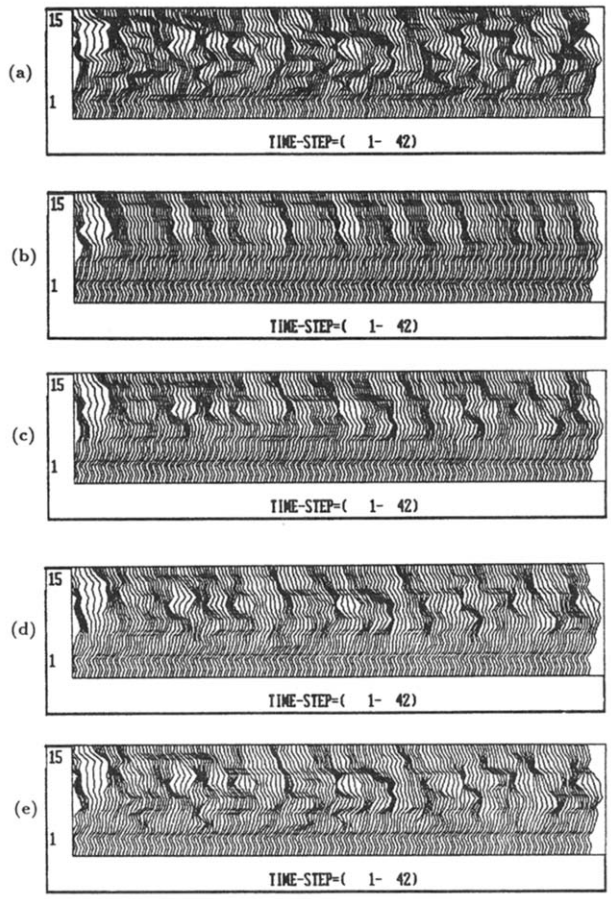

Figure 17. Pseudo-flow visualizations of the reconstructed instantaneous signals. (*a*) Original; (*b*) first eigenmode; (*c*) three eigenmodes; (*d*) five eigenmodes; (*e*) seven eigenmodes.

RESOLUTION REQUIREMENTS

Overview

This section discusses some of the unique problems encountered in the interpretation of multipoint measurements. It should be obvious that the aggregate of the measurements can be no better than each of them individually. Thus, regardless of whether the data are taken simultaneously at many points simply to expedite the collection of single-point data or because additional information is sought on the spatial characteristics of the field, the spatial, temporal, and dynamic range requirements for each probe are the same as for single-point measuring techniques. (Reference [27] summarizes these requirements for turbulence measurement.) In brief:

- The dynamic range of the probe, calibration, and supporting instrumentation must cover the appropriate range of the signals encountered at each location. Note that what dynamic range is appropriate is very much a function of what information is to be

sought. Generally, the greater the dependence on the higher moments of the signal, the greater the dynamical range required.

- The spatial resolution must be adequate so that the information removed by the averaging over the measurement area (or probe volume) is within acceptable limits. Again, what is acceptable spatial filtering is a function of the dependence of the information to be gleaned from the signal on the smallest dynamical scales of the flow. A general guideline is that the largest dimension of the measurement volume (or area) must be less than about half the smallest scale that must be resolved.
- The temporal resolution of the probe and supporting instrumentation must be sufficient to capture the highest frequencies (or transient events) that are of interest. Often these limits are imposed by the physical principles governing the measurement device.

Additional constraints must be imposed on the data acquisition if the data are to be digitized:

- All channels should be sampled simultaneously to avoid introducing phase errors. This is usually accomplished by sample-and-hold amplifiers on each channel. Alternatively, in some situations the phase differences are irrelevant for the intended purpose of the data or can be corrected for after they are transformed to Fourier space.
- The resolution of the A/D converter must be sufficient to minimize the quantization noise to acceptable levels, what is acceptable depending on the information to be sought.
- The sampling rate of the A/D converter must be adequate to ensure that the sampled data can faithfully reproduce the desired information.

These last three criteria defy general guidelines because they are so strongly dependent on what information is desired from the recorded data. Quantization noise is generally white in character and thus most adversely affects those quantities that are dependent on the lowest spectral levels of a signal. This most commonly occurs in turbulence at the highest frequencies (since the turbulence spectra drop off rapidly there) and can cause serious errors in any measurement that depends on the dissipative scales of the flow.

Sampling rate criteria are probably the most familiar of all the experiment design considerations, but they are also the most often misapplied. If (and only if!) it is important to retain the spectral character of the signal in the recorded data (as opposed to simply amplitude information), then the data must be sampled at a rate greater than twice that of the highest frequency present in the signal to avoid aliasing information from one frequency to another. This is the familiar Nyquist criterion and will be seen to have its counterpart in the spatial considerations discussed below. However, if the desired information can be obtained only by reconstructing the instantaneous signal from the digital data (as in many conditional sampling experiments), then the required sampling rate may be as much as 5–10 times higher than the Nyquist criterion would indicate. This is because the reconstruction is carried out for a finite record length signal for which the Whitaker interpolation formula does not apply [28], and usually by less efficient reconstruction algorithms. On the other hand, there are many questions that can be asked about the data (like, what are its statistical moments?) where aliasing is not a problem, and sampling rates substantially lower than the Nyquist rate can and should be used [29].

Finally, there are two additional considerations that affect the length of record and the quantity of data, the first applying to spectral estimation (or other processes related to it) and the second to all estimates of randomly varying data. The latter in essence requires that sufficient independent estimates of any statistical quantity be available to ensure statistical convergence. The former has nothing to do with statistical considerations but arises from the fact that the Fourier transform of a finite record of a signal is actually the convolution of the signal transform with the transform of the record "window." If the record length is not much longer than the longest time scale of the signal, the "spectral leakage" due to the window will adversely affect the spectral character of the recorded signal. This can, of course, affect any inference from the data that depends on its spectral character. Both of these have been discussed in some detail in many places [28, 29].

To exploit the full potential of multipoint measurement techniques for the exploration of the spatial (or spatial and temporal) character of the instantaneous fields, there are additional considerations that must be applied to the design of the spatial arrays. It will be assumed hereafter that all of the concerns addressed above for single-point measurements have been satisfied, and attention will hereafter be focused on the unique aspects of multipoint experimental design.

Periodic and Homogeneous Fields

Spatial resolution requirements for periodic or statistically homogeneous fields are most naturally discussed in terms of a Fourier decomposition, which can be shown to provide an optimal representation [23]. It must be noted that it matters not whether or not it is the intent of the experimenter to spatially Fourier decompose the results of the measurements. Any attempt to reconstruct the field or to analyze the measurements by techniques that depend on spatial variations within it depends implicitly on the Fourier coefficients that constitute it. Thus the multipoint measurements must be performed with sufficient spatial resolution and extent to faithfully capture them.

For periodic fields, the appropriate eigenfunctions are given by $\exp(-\mathrm{i}m\theta)$, where $m = \pm 1, 2, \ldots$, and the corresponding Fourier coefficients by

$$a_m = \frac{1}{2\pi}\int_0^{2\pi} u(\theta) e^{-im\theta}\, d\theta \tag{17}$$

From these, the field can be reconstructed using

$$u(\theta) = \sum_{m=-\infty}^{\infty} a_m e^{im\theta} \tag{18}$$

The number of Fourier modes that can be obtained is, in practice, limited to half the number of points at which the measurements are taken plus one. (The factor 1/2 is

needed because the Fourier coefficients are complex; the extra coefficient is $m = 0$, which is computed from the average of all the data points.) This is exactly the spatial counterpart of the representation of digitally sampled periodic signals by Fourier series.

For statistically homogeneous fields, a Fourier decomposition is also appropriate, except that the *mode number* m is replaced by the *wavenumber* k, which can take any value on the interval $(-\infty, +\infty)$. Because the field is (by definition) of infinite extent, the Fourier coefficient becomes the Fourier transform given by

$$\hat{u}(k) = \int_{-\infty}^{\infty} u(x)e^{-ikx}\,dx \tag{19}$$

The reconstructed field is now given by

$$u(x) = \int_{-\infty}^{\infty} \hat{u}(k)e^{ikx}\,dk \tag{20}$$

From an experimental point of view, the difference between the Fourier series and the Fourier transform vanishes because the measurement field is always of finite extent and the number of measurements is finite. The finite extent limits the lowest (or fundamental) wavenumber to $2\pi/L$, where L is the extent of the measurements, while the finite number of measurement locations restricts the number of independent Fourier coefficients to half the number of measurement points. These are usually evaluated at integer multiples of the fundamental. This is, of course, exactly analogous to the Fourier decomposition of statistically stationary temporally varying signals.

A consequence of discretely sampling the signal in space is that (like its counterpart in time series analysis) the information at one mode (or wavenumber) can be aliased into lower modes. This is most easily demonstrated for samples taken at equally spaced distance intervals. Suppose M modes are required to represent the signal and only $N/2$ modes can be computed (from N measurement locations). Then when $M > N/2$, the information in the mth mode for $m > N/2$ (but less than N) appears in the calculated $(N - m)$th mode. If $m > N$ (but less than $3N/2$), it is aliased to the $(m - N)$th mode, and so on (see Fig. 19 for $N = 30$ case). It is important to note that once the data is aliased, there is no way to unalias it, and the modal composition of the original signal is irretrievable.

If the spectral content (mean-square Fourier coefficients) of the signal is varying monotonically and dropping rapidly as the mode number increases, the effects of aliasing may be negligible. This is often the case in measurement of one-dimensional turbulence spectra (usually inferred from temporal spectra), which always have significant spectral content at very low wavenumber and often peak there. On the other hand, modal analysis of spatially sampled data can and often does lead to situations where the spectral content of the lowest modes can be small compared to that of the higher modes. When this occurs, even a relatively high number of resolved modes (compared to that of the peak) can lead to significant aliasing of the lowest modes.

Figure 18 from Ref. [30] shows a modal decomposition of the mixing layer of an axisymmetric jet using 30 and 48 positions around the circle. Note the apparent modal

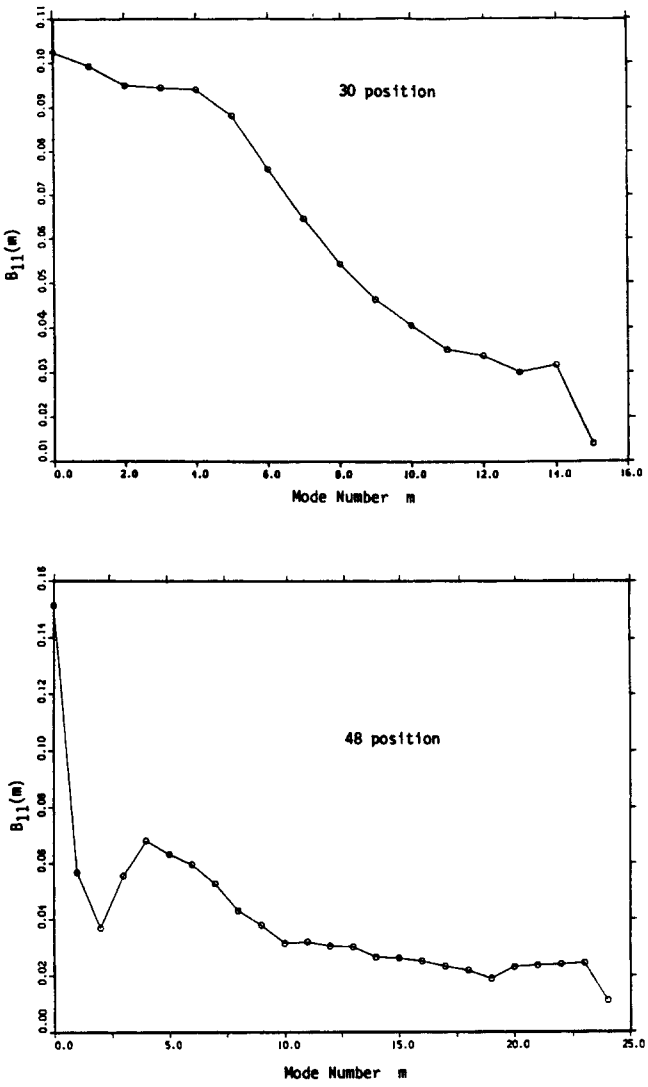

Figure 18. Modal decomposition of the mixing layer of an axisymmetric jet using both 30 and 48 positions around the circle.

content in the first few modes of the 30-position data, which is reduced when the circle is resolved by 48 positions. It can be shown by arguing that the spectra fall off smoothly at the higher modes (in fact, as $m^{-5/3}$) that the low-mode-number peak is largely due to aliasing. This is substantiated by the Nyquist diagram of Fig. 19 for the 30-position case, which shows where the information above mode 16 is aliased. Clearly the physical processes inferred from the aliased data would be quite different from those actually present.

Aliasing in temporal data analysis can be minimized (and sometimes avoided entirely) by low-pass filtering *before digitizing* to remove the Fourier content at frequencies above half the sampling rate. The counterpart for spatial sampling would be *spatial low-pass filtering*. The concept, if primitively applied, would necessitate using many probes closely enough spaced to allow resolution of all the modes, then smoothing adjacent probe data samples to remove the highest modes or wavenumbers. This is not possible in most applications because of practical

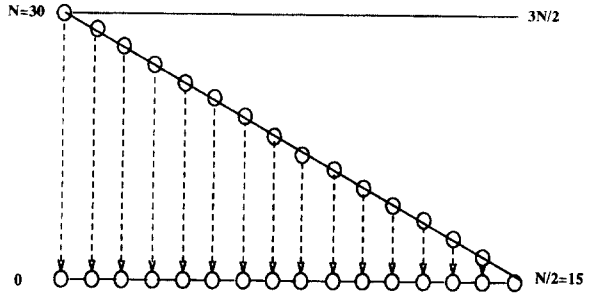

Figure 19. Nyquist diagram for the 30-position case showing where the information above mode 16 is aliased.

limitations on the number of probes and on how closely they can be spaced. As a consequence, most experiments to date have simply ignored the aliasing problem and hoped it wasn't there, sometimes with very misleading results!

Ironically, the spatial aliasing problem can be addressed in a straightforward manner by exploiting to advantage one of the principal limitations on single-point measurements, namely, the unavoidable spatial filtering arising from the finite spatial extent of the probe. By making the probe dimensions (eg, the sensing wire length) large enough to span the distance between the measurement sites, the resulting spatial filtering removes the Fourier content of the modes that would have otherwise been aliased. Note that an analogous type of temporal filtering was implemented before the advent of modern high capture rate A/D converters by averaging the signal across the entire interval between sample times (L. Kristensen, RISOE, Roskilde, Denmark, private communication, 1980).

A less satisfactory alternative than direct spatial filtering is to use the interrelation of spatial and temporal disturbances in many fields, especially turbulence. The temporal fluctuations in a convected spatial field are due only in part to the unsteadiness in the field ($\partial/\partial t$), the remaining part arising from the spatial variations in the field being swept by the probe ($U_c\,\partial/\partial x$, where U_c is the effective convection velocity). If the turbulence intensity is low, the convected spatial disturbances can dominate the unsteady signal. When this happens, there is a correlation between the frequency of the disturbance seen by the probe, say f, and the size of the disturbance, say β. Thus it is possible to remove at least a portion of the spatial information smaller than a given wavelength, say β_0, by temporally low-pass filtering the data above $f_0 = U_c/\beta_0$.

The finite extent of the measurement field imposes a spatial window on the data exactly as does the finite length of record in time. If the measurements are performed between $-L/2$ and, $L/2$, the spectral window

$$W(k) = L\frac{\sin(\pi kL)}{\pi kL} \tag{21}$$

is convolved with the measurements. Although this does not cause any change in the validity of the data itself (ie, each individual data point), it does adversely affect the determination of which Fourier coefficients comprise it. The problem is exactly analogous to the window problems resulting from the finite record length of temporal signals. In general, the smaller the spatial extent of the measurements relative to the scale of the disturbances containing the energy and the more rapidly the spectrum falls off with wavenumber, the greater the adverse effects of the resulting spectral leakage. Note that if the spectrum peaks away from the origin, the leakage can be in both directions away from the peak. This is, of course, not a problem for periodic fields (like those that have axial symmetry) as long as the entire field is considered, but it is a problem for homogeneous or locally homogeneous fields where only a portion of the field can be considered.

Inhomogeneous Fields

The establishment of criteria to govern the spatial sampling of inhomogeneous fields is of great importance because most engineering flows are strongly inhomogeneous in one or more directions. As for the homogeneous or periodic flows discussed above, the problem of deciding how many probes to use, where they should be placed, what their spacing should be, and how much of the flow they should span is obviously crucial to the successful inference of flow structure from the measurements. These questions represent a substantial challenge, in part because, unlike homogeneous or periodic flows, there is no convenient and general counterpart to the analytical Fourier modes from which the conclusions of the previous sections were drawn. Clearly, ideas like aliasing and spectral leakage must have their counterpart in the sampling of inhomogeneous fields as well, even though they are not well represented by Fourier modes.

To quantify the problems, it is necessary either to choose particular fields or to select a means of representing a variety of them. The proper orthogonal decomposition discussed earlier is a natural candidate for this discussion, both because it is a general method applicable to all inhomogeneous flows (it reduces to the Fourier decomposition for homogeneous or periodic flows) and because it is of interest in its own right (as evidenced by the activities discussed earlier). Whether one is interested in the POD or not, because it provides an optimal representation of the flow (in terms of capturing its energy with the fewest terms), it is hard to imagine that any other way of looking at the spatial characteristics of the field would have less stringent requirements.

For the purpose of this discussion, attention will be focused on the one-dimensional decomposition posed by

$$\int_{\text{region}} R(x,x')\phi^n(x')\,dx' = \lambda_n\phi^n(x) \tag{22}$$

where ϕ^n is the nth eigenfunction, λ_n is the corresponding eigenvector, and $R(x,x')$ is the two-point correlation given by

$$R(x,x') = \langle u(x)u(x')\rangle \tag{23}$$

For real fields, both the eigenvalues and eigenfunctions are real, and the latter are orthogonal and can be chosen to be orthonormal. The decomposition is optimal in that the lowest order eigenvalue is the largest, the next one is

next largest, and so forth, so that the representation requires the fewest terms of any decomposition to represent the field.

A random field can be reconstructed from the eigenfunctions using

$$u(x) = \sum_{n=1}^{\infty} a_n \phi^n(x) \tag{24}$$

where the coefficients a_n are random, in general, and satisfy

$$\langle a_n a_m \rangle = \lambda_n \delta_{mn} \tag{25}$$

For a single realization of the random field, the coefficients are given by

$$a_n = \int_{\text{region}} u(x)\phi^n(x)\, dx \tag{26}$$

It is easy to show that the two-point correlation can be recovered by

$$R(x, x') = \sum_{i=1}^{\infty} \lambda_n \phi^n(x)\phi^n(x') \tag{27}$$

If the objective of the multipoint measurements is to determine the eigenfunctions and eigenvalues from experimentally determined values of the two-point correlation $R(x, x')$, then the problem reduces to obtaining sufficient data to solve numerically the integral of Eq. (22). The accurate determination of $R(x, x')$ is, of course, also a problem, but one of the type discussed in the overview section. The problem of interest here is the measurement grid: How many points are required, and where should they be located? Although the Nyguist and window criteria of the preceding section would certainly be adequate (because the field can be expanded in Fourier modes, although less optimally), there are probably substantially less stringent requirements that will suffice. Very little work has been done to determine what these criteria might be, and experimenters have largely relied on intuition and empirical tests. The following paragraphs attempt to summarize current understanding and set forth at least the beginnings of a sampling theory for inhomogeneous flows. The two questions of quantity and location will be considered separately, beginning with the former.

It is obvious that the number of measurement locations in any experiment must be finite. Therefore the integral equation (22) must be approximated by the matrix equation

$$R_{ij}\phi_j = \lambda\phi_i \tag{28}$$

The subscripts $i, j = 1, \ldots, N$ represent the measurement points, and R_{ij} represents the correlation computed at pairs of these locations, that is,

$$R_{ij} = \langle u_i u_j \rangle \tag{29}$$

(Note that in practice R_{ij} is replaced by a more complicated matrix using appropriate weighting factors to ensure that it is symmetric [24].) The techniques for solving this equivalent matrix eigenvalue problem are well documented in many places (see Refs. [24] and [31] for particularly relevant discussions). Of primary importance here is the fact that at most N linearly independent solutions exist corresponding to the N eigenvalues. Thus the number of measurement locations determines the maximum number of eigenfunctions that can be obtained. To see how many measurement locations are required, it is useful to hypothesize that a field is *mode-limited*, which is defined to mean that all modes above a given number, say M, are identically zero. It is obvious from the above that the field can be properly resolved only if $N \geq M$. If $N > M$, then the first M eigenvalues necessary to specify the field will be determined, and the extra $N - M$ eigenvalues will be zero. On the other hand, if $N \leq M$, the eigenvalues determined will not correspond uniquely to those of the original field but will have additional information from those eigenvalues for $M > N$ "leaked" into them. This can most easily be demonstrated by attempting to determine a three-mode field using only two locations. The two eigenvalues that can be determined are functions of all three eigenvalues actually present. Figure 20 from Glauser et al [30] shows different results for a jet mixing layer using seven- and 13-wire configurations. The differences are due in part to the aliasing of unresolved modes in the seven-wire case and in part to the better approximation to the integral of Eq. (22) for the 13-wire case.

Lumley [32] argues that the number of terms required to capture most of the energy is proportional to the spatial extent of the inhomogeneity divided by the integral scale of the field, that is, L_{in}/l. In the Glauser–George experiment, this number is about 3–5 and corresponds closely to the number of terms that proved to be significant in their experiment. For boundary layer flows, the integral scale is a strong function of distance from the wall in the near-wall region. Thus, if the entire flow domain is used, the number of required terms can be quite large as discussed below. On the other hand, subdomains can be used to reduce the domain—one eliminating the near-wall region where the integral scale is small, and another including only the near-wall region so that the domain is small. The result is that the required number of terms is smaller for each subdomain. Note that although this works for capturing the turbulence energy, it does not imply that the higher terms may not be important for other kinds of processing like conditional sampling.

The discussion above can be illustrated by the results of Chambers et al [33] and Moin and Moser [31], who used numerical simulations to study how the domain over which the integral is computed affects the resulting eigenvalues. For the boundary layer type flows they investigated, integration over the entire domain yielded a substantially larger number of eigenfunctions than did integration over subdomains consisting of the near-wall region only and a region comprising most of the flow excluding the near-wall region. In both of these situations, the inner–outer character of the flow lends itself naturally to this kind of splitting of the problem. Presumably a proper interpretation of the decomposition for each regime would seek influences of one region on the other, perhaps through the coupling of the pressure field between them. No such physical reasons are available for splitting the jet mixing layer flow of Glauser et al [30], where the largest scales dominate the entire flow. The important message from these results is that regardless of the domain chose, it will likely influence greatly the modal character of the recon-

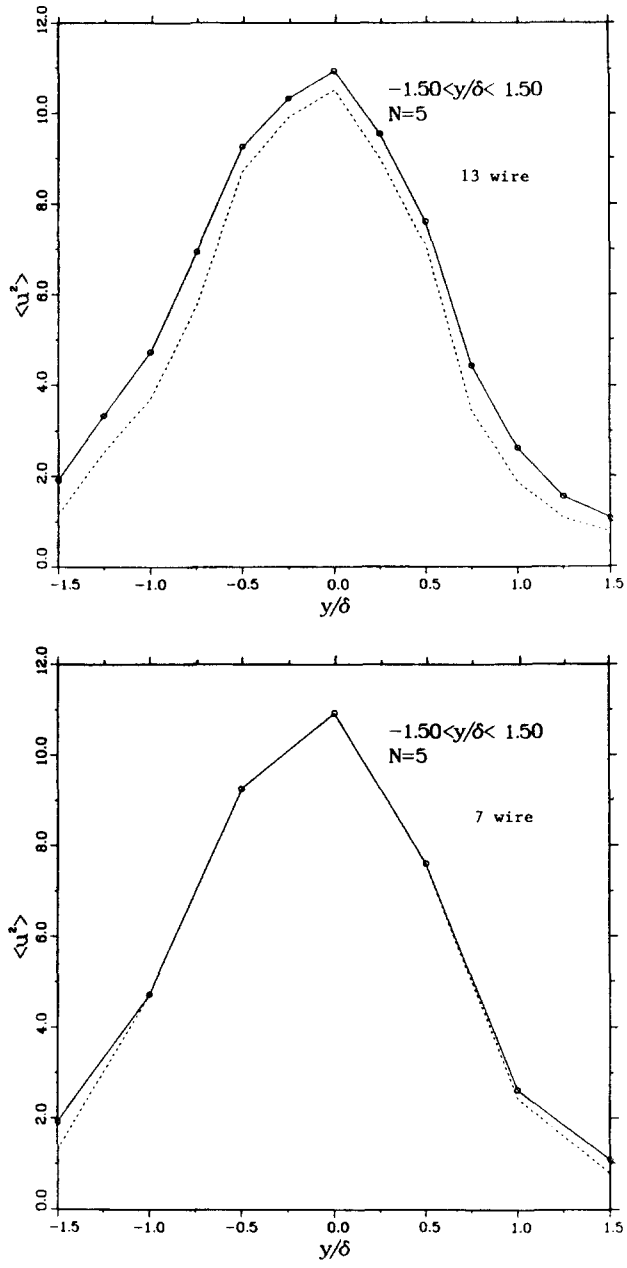

Figure 20. Five-mode convergence comparison of streamwise component of kinetic energy for a jet mixing layer using seven- and 13-wire configurations. Note how the seven-wire case converges more rapidly.

structed field and most probably any inferences drawn from it.

Usually one cannot guarantee that modes above a certain number are not present unless they are removed by spatial filtering, perhaps of the type discussed in the preceding section. In the absence of detailed knowledge about the eigenfunctions, it is not possible to state precisely how such filtering should be carried out. It has been noted, however, by a number of investigators (eg, Chambers et al [33] and Moin and Moser [31]) that the higher the mode number, the more closely the eigenfunctions resemble Fourier modes. Thus, the criteria for homogeneous (in this case, locally homogeneous) flows provide useful guidelines.

Even if the number of measurement locations and the spatial extent of the measurement field are sufficient to satisfy the concerns cited above, that alone does not ensure that the eigenvalues and eigenvectors determined from the matrix equation [Eq. (28)] correspond to those of the original integral equation [Eq. (22)]. The most difficult question of all is to determine in advance (without already knowing the eigenfunctions) where the measurements should be taken to ensure the best (or even an adequate) approximation to the real integral eigenvalue problem of Eq. (22). Certainly it would seem reasonable to concentrate the measurement grid in regions where the kernel, $R(x, x')$, is changing most rapidly, if care is taken to weight the matrix elements so as to not artificially redistribute the energy. This is the same kind of logic that lies behind the logarithmic spacing often used in boundary layer studies.

Some further insight into where the measurement points should be located (as well as some justification for the qualitative argument above) can be obtained by examining Lumley's [32] method of calculation by successive approximation where the $(n + 1)$th approximation, say $\phi^{(n+1)}$, is related to the nth, $\phi^{(n)}$, approximation by

$$\int_{\text{region}} R(x, x')\phi^{(n)}(x')\,dx' = \phi^{(n+1)} \tag{30}$$

where the first eigenvalue is obtained from

$$\frac{\phi_1^{(n+1)}}{\phi_1^{(n)}} \to \lambda_1 \tag{31}$$

and the first eigenfunction from

$$\frac{\phi_1^{(n)}}{\lambda_1} \to \phi_1 \int_{\text{region}} \phi_1 {}^{*}\phi_1^{0*}\,dx \tag{32}$$

If the first "guess" is taken as $\phi_1^0 = 1$, then it is easy to see that the measurement locations must be chosen so that the integral of $R(x, x')$ over x' is correctly computed. There is no reason, in general, to believe that the best choice of locations for estimating the eigenvalues at one value of x will be the best for all. In view of this and in the absence of other information, a uniformly spaced grid might be the best compromise. Also, in the absence of more specific criteria, the current approach of halving (or doubling) the resolution to see how the eigenvalues change is perhaps the only way to confirm that the choices of grid are correct.

While the considerations above may ensure the correct behavior of the lowest modes, the higher modes may still present problems. This can also be seen from Lumley's method where the $(n + 1)$th mode is calculated from the kernel minus its reconstruction from the first n modes; that is,

$$\int_{\text{region}} \left[R(x, x') - \sum_{k=1}^{n} \lambda_k \phi^k(x)\phi^k(x') \right] \phi_{(n+1)}^{(m)}(x')\,dx' = \phi_{(n+1)}^{(m+1)}(x) \tag{33}$$

It is obvious that the higher the mode number to be calculated, the more it depends on the cumulative errors in the lower modes. These conclusions do not depend on the method of successive approximations but are general in that the errors will be most pronounced in the higher modes.

SUMMARY AND CONCLUSIONS

Simultaneous multipoint measurements have been shown (both here and elsewhere) to provide unique tools for aiding in the understanding of turbulence structure in ways not possible with single-point measurements. Several examples have been briefly reviewed that demonstrate how such measurements have helped shed new light on the turbulence structure in wakes, jets, free shear layers, channel flow, and boundary layers. The interpretation of the data obtained with the rakes has been enhanced by using conditional averages, pseudo-flow visualization, stochastic estimation, and the proper orthogonal decomposition.

The problem of multipoint measurements has been shown to be much greater than one of simply designing and building impressive arrays of probes that do not by their presence change the flow. An attempt has been made to make clear that there are a number of serious questions that must be addressed before spatially sampled data can be used to infer spatial and temporal structure in the flow. An obvious constraint that must be met is that spatial, temporal, and dynamic range requirements for *each* probe on the rake are the same as for single-point measuring techniques. To exploit the full potential of multipoint techniques for extraction of the spatial character of the instantaneous fields, however, there are additional considerations that must be applied to their design. With the aid of Fourier analysis for periodic and statistically homogeneous fields, spatial aliasing and spectral windowing are shown to be concerns that must be dealt with, just as they are in digital time series analysis. An idea is proposed for *spatial low-pass filtering*, which involves exploiting to advantage the spatial filtering arising from the finite spatial extent of the probe. An attempt has also been made, using the proper orthogonal decomposition, to establish criteria that govern the spatial sampling of inhomogeneous fields because ideas like aliasing and spectral leakage have their counterpart here as well. It is argued that the criteria established for homogeneous fields would certainly be adequate for inhomogeneous fields, but these are probably more stringent than is actually required.

It has been noted that Fourier techniques and proper orthogonal decomposition were used both to establish general sampling criteria and because they are of interest in their own right. Thus, even if it is not the intent of the experimenter to use these techniques to decompose the measurements, *multipoint measurements must still be performed over a sufficient span and with sufficient spatial resolution (or appropriate spatial low-pass filtering applied) so as to avoid spatial aliasing and windowing effects*. This is especially true when inferences are to be drawn from gradients computed from the instantaneous signals (eg, vorticity).

PRACTICAL SIGNIFICANCE AND FUTURE APPLICATIONS

Although the ideas discussed here have been developed for turbulent velocity fields, the advantages of multipoint measurements are obvious for other variables such as pressure and temperature and the various kinds of flow situations in which they occur. Although the examples used herein have been entirely drawn from experiments using rakes of hot wires, the techniques used to analyze the measurements and the resolution criteria governing them are applicable to all types of transducers. With the rapid advancement of modern optical techniques for flow measurement, there is good reason to believe that multipoint measurement techniques will find increasing application in both scientific and engineering investigations. If care is taken to address the concerns expressed in this paper, the increased physical insight and understanding resulting from them should be substantial.

The ideas expressed in this paper were not developed in isolation but have evolved over many years of discussions and interactions with a number of people. At the risk of leaving someone out, we would particularly like to acknowledge Professors R. Adrian, N. Aubry, Y. Guezennec, S. Herzog, J. Lumley, and P. Moin, Dr. J. P. Bonnet, Dr. S. Leib, and Dr. R. Moser. MNG would also like to thank the National Science Foundation, under grants MSM-8808872 and INT-9016045, Dr. Aldo Peracchio of Pratt and Whitney/UTC, and the Cornell-Clarkson NASA Space Grant Consortia for funding portions of this work.

REFERENCES

1. National Committee for Fluid Mechanics Films, *Illustrated Experiments in Fluid Mechanics*, distributed by Encyclopaedia Brittanica Educational Corp., Chicago, Ill., 1972.
2. Van Dyke, M., *An Album of Fluid Motion*, Parabolic Press, Stanford, Calif., 1982.
3. Blackwelder, R. F., and Kaplan, R. E., On the Wall Structure of the Turbulent Boundary Layer, *J. Fluid Mech*, **76**, 89–118, 1976.
4. Teitel, M., and Antonia, R. A., The Interaction Region of a Turbulent Duct Flow, *Phys. Fluids A*, **2**(5), 808–813, 1990.
5. Antonia, R. A., Browne, L. W. B., and Bisset, D. K., Symmetric and Antisymmetric Modes in the Turbulent Far-Wake, Sixth Symposium on Turbulent Shear Flows, Toulouse, France, 10-3-1–10-3-5, 1987.
6. Browand, F. K., and Troutt, T. R., A Note on Spanwise Structure in the Two-Dimensional Mixing Layer, *J. Fluid Mech.*, **97**, 771–781, 1980.
7. Hussain, A. K. M. F., Coherent Structures—Reality and Myth, *Phys. Fluids*, **26**, 2816–2850, 1983.
8. Tabatabai, M., Kawall, J. G., and Keffer, J. F., Flow Visualisation Using Hot-Wire Anemometry, Dantec Information No. 04, February 1987.
9. Delville, J., Bellin, S., Garem, J. H., and Bonnet, J. P., Analysis of Structures in a Turbulent Plane Mixing Layer by Use of a Pseudo Flow Visualization Method Based on Hot-Wire Anemometry, in *Advances in Turbulence II*, H. H. Fernholtz and H. E. Fiedler, Eds., pp. 251–256, Springer-Verlag, New York, 1988.
10. Lumley, J. L., On the Interpretation of Time Spectra Measured in High Intensity Shear Flows, *Phys. Fluids*, **8**, 1056, 1965.
11. Zaman, K. B. M. Q., and Hussain, A. K. M. F., Taylor's Hypothesis and Large-Scale Coherent Structures, *J. Fluid Mech.*, **112**, 379–396, 1981.
12. Ukeiley, L., Wick, D., and Glauser, M., Coherent Structure

Identification in a Lobed Mixer, ASME paper 91-GT-307, 1991.
13. Ukeiley, L., Wick, D., and Glauser, M., A Novel Hot-Wire Rake Design, ASME FED- Vol. 97, pp. 87–92, ASME, New York, 1990.
14. Eckerle, W. A., Sheibani, H., and Awad, J., Experimental Measurements of the Vortex Development Downstream of a Lobed Forced Mixer, ASME paper 90-GT-27, 1990.
15. Adrian, R. J., and Moin, P., Stochastic Estimation of Organized Turbulent Structure: Homogeneous Shear Flow, *J. Fluid Mech.*, **190**, 531–559, 1988.
16. Tung, T. C., and Adrian, R. J., Higher-Order Estimates of Conditional Eddies in Isotropic Turbulence, *Phys. Fluids*, **23**, 1469–1470, 1980.
17. Adrian, R. J., On the Role of Conditional Averages in Turbulence Theory, in *Turbulence in Liquids*, pp. 323–332, Science Press, Princeton, N.J., 1977.
18. Cole, D., Glauser, M., and Guezennec, Y., Stochastic Estimation Applied to the Axisymmetric Jet Mixing Layer, *Bull. Am. Phys. Soc.*, **35**(10), 2312–2313, 1990.
19. Cole, D., Glauser, M., and Guezennec, Y., Stochastic Estimation Applied to the Axisymmetric Jet Mixing Layer, *Phys. Fluids A*, **4**(1), 192–194, 1992.
20. Glauser, M. N., and George, W. K., An Orthogonal Decomposition of the Axisymmetric Jet Mixing Layer Utilizing Cross-Wire Velocity Measurements, Sixth Symposium on Turbulent Shear Flows, pp. 10-1-1–10-1-6, Toulouse, France, 1987.
21. Glauser, M. N., Coherent Structures in the Axisymmetric Turbulent Jet Shear Layer, Ph.D. Thesis, State University of New York at Buffalo, 1987.
22. Lumley, J. L., The Structure of Inhomogeneous Turbulent Flows, in *Atmospheric Turbulence and Radio Wave Propagation*, A. M. Yaglom and V. I. Tatarsky, Eds., Nauka, Moscow, pp. 166–178, 1967 (in English).
23. George, W. K., Insight into the Dynamics of Coherent Structures from a Proper Orthogonal Decomposition, Symposium on Near Wall Turbulence, Dubrovnik, Yugoslavia, May 16–20, 1988.
24. Glauser, M. N., Leib, S. J., and George, W. K., Coherent Structures in the Axisymmetric Jet Mixing Layer, *Turbul. Shear Flows*, **5**, Springer Verlag, 134–145, 1987.
25. Aubry, N., Holmes, P., Lumley, J. L., and Stone, E., The Dynamics of Coherent Structures in the Wall Region of a Turbulent Boundary Layer, *J. Fluid Mech.*, **192**, 115–173, 1988.
26. Glauser, M. N., Zheng, X., and Doering, C. R., The Dynamics of Organized Structures in the Axisymmetric Jet Mixing Layer, in *Turbulence and Coherent Structures*, M. Lesieur and O. Metais, Eds., pp. 253–265, Kluwer, Boston, 1991.
27. George, W. K., and Taulbee, D., Designing Experiments to Test Closure Hypotheses, in *Engineering Turbulence Modeling and Experiments*, W. Rodi and E. N. Ganic, Eds., pp. 383–397, Elsevier, New York, 1990.
28. Tan-atichat, J., and George, W. K., Use of Computer of Data Acquisition and Processing, in *Handbook of Fluids and Fluid Machinery*, A. E. Fuhs, Ed., Wiley, New York, 1985.
29. George, W. K., Processing of Random Signals, Dynamic Flow Conference, pp. 757–800, Skovlunde, Denmark, 1978.
30. Glauser, M. N., Zheng, X., and George, W. K., An Analysis of the Turbulent Axisymmetric Jet Mixing Layer Utilizing Proper Orthogonal Decomposition, 1992, submitted.
31. Moin, P., and Moser, R. D., Characteristic-Eddy Decomposition of Turbulence in a Channel, *J. Fluid Mech.*, **200**, 471–509, 1989.
32. Lumley, J. L., *Stochastic Tools in Turbulence*, Academic, New York, 1970.
33. Chambers, D. H., Adrian, R. J., Moin, P., Stewart, D. S., and Sung, H. J., Karhunen–Loeve Expansion of Burgers' Model of Turbulence, *Phys. Fluids*, **31**, 2573–2582, 1988.

Received August 14, 1991; revised January 13, 1992